A Grand Scan of the pMSSM Parameter Space for Snowmass 2021

Jennet Dickinson[1], Samuel Bein[2], Sven Heinemeyer[3], Joshua Hiltbrand[4], Jim Hirschauer[1], Walter Hopkins[6], Elliot Lipeles[5], Malte Mrowietz[2], and Nadja Strobbe[4]

[1]Fermi National Accelerator Laboratory
[2]University of Hamburg
[3]Instituto de Física Teórica (UAM/CSIC), Universidad Autónoma de Madrid, Cantoblanco, 28049, Madrid, Spain
[4]University of Minnesota
[5]University of Pennsylvania
[6]Argonne National Laboratory

March 2022

1 Introduction

It is well known that the Standard Model of particle physics (SM) cannot be the ultimate theory of fundamental particles and interactions. Most obviously, the SM does not incorporate gravity and explains neither the identity of the astronomically observed dark matter (DM) nor the observed multiplicities and hierarchies of interactions, flavor, and fermion generations. Of the many models proposed to address the shortcomings of the SM, supersymmetry (SUSY) garners significant interest because it simultaneously explains the finite mass of the recently discovered Higgs particle, provides a DM candidate, and allows more precise unification of the forces.

The minimal supersymmetric standard model (MSSM) [1–5] has 105 parameters (in addition to the SM parameters) describing particle masses and interactions. In order to facilitate interpretation of experimental results within the MSSM framework, there are two main possibilities to deal with this large number of free parameters. One consists in assuming unification at some high scale, at which a certain soft SUSY-breaking mechanism is adopted. This can reduce the number of free parameters to as few as five, depending on the mechanism responsible for the values of the new particles' masses, referred to as the soft SUSY breaking mechanism. The most prominent example is the "Constrained MSSM" (cMSSM) [6–9]. Another assumes the production of one set of SUSY particles at the electroweak (EW) scale with a fixed decay chain. This approach is called "simplified model spectra" (SMS) approach [10–12]. While these frameworks allow for efficient interpretation of results, they do so at the expense of sampling only a very small part of the phase space of the MSSM and potentially focus on signatures that may not be realized in nature.

In the past years, the ATLAS and CMS collaborations [13, 14] and theorists have attempted to ameliorate the limitations of interpretations based on the cMSSM and SMS by using the phenomenological MSSM (pMSSM)[15–20]. The pMSSM reduces the full MSSM space to nineteen free parameters, specified at the electroweak (EW) scale, based on assumptions consistent with current experimental constraints rather than details of the soft SUSY breaking mechanism. The parameters of the pMSSM and their definitions are listed in Table 1.

Building on the methods of the CMS and ATLAS collaborations, we have developed a flexible framework for interpretation of SUSY sensitivity studies for future colliders in the framework of the pMSSM. We perform a *grand scan* of the pMSSM parameter space that covers the logical OR of accessible ranges of many collider scenarios, including electron, muon, and hadron colliders at a variety of center of mass energies. This enables comparisons of sensitivity and complementarity of different future experiments, including both colliders and precision measurements in the Cosmological and Rare Frontiers. The pMSSM parameter ranges considered

Param.	Definition	Range	Sampling
M_A	mass of psuedoscalar Higgs boson	100 GeV - 25 TeV	Log
$\tan\beta$	ratio of Higgs vevs	1 - 60	Log
$\lvert\mu\rvert$	Higgs-higgsino mass parameter	80 GeV - 25 TeV	Log
$\lvert M_1\rvert$	bino mass parameter	1 GeV - 25 TeV	Log
$\lvert M_2\rvert$	wino mass parameter	70 GeV - 25 TeV	Log
M_3	gluino mass parameter	200 GeV - 50 TeV	Linear
$m_{\tilde{L}^{1,2}}$	$1^{\text{st}}/2^{\text{nd}}$ gen. left-handed slepton mass	90 GeV - 25 TeV	Log
$m_{\tilde{R}^{1,2}}$	$1^{\text{st}}/2^{\text{nd}}$ gen. right-handed slepton mass	90 GeV - 25 TeV	Log
$m_{\tilde{L}^3}$	3^{rd} gen. left-handed slepton mass	90 GeV - 25 TeV	Log
$m_{\tilde{R}^3}$	3^{rd} gen. right-handed slepton mass	90 GeV - 25 TeV	Log
$m_{\tilde{q}^{1,2}}$	$1^{\text{st}}/2^{\text{nd}}$ gen. left-handed squark mass	200 GeV - 50 TeV	Linear
$m_{\tilde{u}^{1,2}}$	$1^{\text{st}}/2^{\text{nd}}$ gen. right-handed u-type squark mass	200 GeV - 50 TeV	Linear
$m_{\tilde{d}^{1,2}}$	$1^{\text{st}}/2^{\text{nd}}$ gen. right-handed d-type squark mass	200 GeV - 50 TeV	Linear
$m_{\tilde{q}^3}$	3^{rd} gen. left-handed squark mass	100 GeV - 50 TeV	Linear
$m_{\tilde{u}^3}$	right-handed stop quark mass parameter	100 GeV - 50 TeV	Linear
$m_{\tilde{d}^3}$	right-handed sbottom quark mass parameter	100 GeV - 50 TeV	Linear
$\lvert A_\tau\rvert$	τ trilinear coupling	1 GeV - 7 TeV	Log
$\lvert A_b\rvert$	bottom trilinear coupling	1 GeV - 7 TeV	Log
$\lvert A_t\rvert$	top trilinear coupling	1 GeV - $3(m_{\tilde{q}^3} m_{\tilde{u}^3})^{1/2}$	Log

Table 1: The 19 parameters of the pMSSM and their allowed ranges in the Snowmass 2021 scan. All complex parameters are taken to be real.

are listed in Table 1. The lower bounds on each parameter are chosen based on experimental constraints and phenomelology considerations. The upper bounds are chosen to be within reach of the sensitivity of a 100 TeV proton-proton collider. The top quark mass, bottom quark mass, and strong coupling constant α_S are sampled from a Gaussian distribution centered at the the measured best-fit value listed in Table 2. All other SM parameters are fixed to the measured best-fit values.

SM Param.	Definition	Measurement
m_t	top quark mass	173.1 ± 0.9 GeV
m_b	bottom quark mass	$4.18^{+0.03}_{-0.02}$ GeV
α_s	strong coupling constant	0.1181 ± 0.0011

Table 2: SM parameters that are sampled in the pMSSM scan. All other SM parameters are fixed to the best-fit values.

The output of the scan for each selected point includes the pMSSM and SM parameter values. The SUSY particle masses are calculated by the SPheno 4.0.5 [21, 22] spectrum generator, which also produces an SLHA file [23] for generating signal events for each point. Event generation and detector simulation is not discussed in this whitepaper.

Section 2 describes how the scan is performed by using a Markov chain Monte Carlo procedure to sample points from the 19-dimensional pMSSM parameter space. Section 3 describes how properties of theoretical and experimental interest are calculated for each point. Section 4 reviews the scan coverage in terms of a selection of interesting physics processes and estimates the impact of future precision measurements on the pMSSM phase space. Conclusions and an outlook are given in Section 6.

2 Markov chain Monte Carlo sampling procedure

Due to the high dimensionality of the pMSSM and the large span of the parameter ranges (Table 1), the parameter space considered in this scan is extremely large. A Markov chain Monte Carlo (McMC) [24–28] algorithm is therefore used to explore the space in an efficient way, guided by a likelihood constructed from existing experimental results (see Section 2.1)

To begin the McMC scan, an initial pMSSM point in the 19D parameter space is selected at random within the ranges specified in Table 1. The SPheno spectrum generator is used to calculate the corresponding particle masses and decays. The Higgs sector is then replaced with that calculated by FeynHiggs 2.18.0 [29–36]. If SPheno or FeynHiggs indicate that the selected point is not a valid pMSSM model, e.g., that there is no tachyon present in the spectrum, or the LSP is determined to not be a neutralino, a new random point is selected until a viable initial point is obtained. The McMC likelihood for the initial point is calculated as described in Section 2.1.

The following steps are repeated until the desired number of points is reached:

1. A new pMSSM point $\vec{x}'$ is selected from the previous one ($\vec{x}$) by sampling randomly from the probability distribution given by the stepping functions $f_i(x_i)$, where i is the parameter index. The form of the stepping function is discussed in detail in Section 2.2.

2. If the pMSSM point does not fall within the ranges listed in Table 1, return to step 1.

3. The particle spectrum and Higgs sector quantities for $\vec{x}'$ are calculated with SPheno and FeynHiggs respectively. If the pMSSM point is not a valid model or the uncertainty on the calculated Higgs boson mass is larger than 5 GeV, return to step 1.

4. Perform additional calculations required to compute the McMC likelihood (detailed in Section 2.1).

5. If the likelihood ratio $L(\vec{x}')/L(\vec{x}) > 1$, the point is accepted. If the likelihood ratio satisfies $L(\vec{x}')/L(\vec{x}) \leq 1$, it is compared to a random number n_R in the interval [0,1], and the point is accepted if $L(\vec{x}')/L(\vec{x}) > n_R$ (this allows the McMC to move away from a local minimum). Otherwise, the point is rejected.

6. If the point is rejected, return to step 1.

7. If the point is accepted, save the point. Then take $\vec{x} = \vec{x}'$ and repeat from step 1.

The final pMSSM scan comprises the union of 400 independent McMC scan threads, each starting from a unique random initial point.

2.1 Construction of the likelihood

In order to steer the McMC out of regions of parameter space that are well excluded by existing measurements, a likelihood function is constructed to quantify the compatibility of each generated pMSSM point with the following experimental results:

- Measured branching ratios of $B \to \tau\nu$, $D_s \to \tau\nu$, and $D_s \to \mu\nu$, computed by SPheno 4.0.5;
- Measurements of additional B-physics observables and their correlations, computed with Superiso [37];
- Higgs boson measurements from LEP, the Tevatron, and the LHC (computed with HiggsSignals [38, 39] and HiggsBounds [40–44];
- Measurement of Δa_μ from the muon $g-2$ experiment (in half of scan threads, see below).

The total likelihood is taken to be a product of the contribution from each of these sources.

The branching ratios $B \to \tau\nu$, $D_s \to \tau\nu$, and $D_s \to \mu\nu$ have a Gaussian contribution to the total likelihood, with the mean and width corresponding to the measured value and uncertainties, respectively. The contribution of each observable to the total likelihood is the Gaussian likelihood function evaluated at the value calculated by SPheno.

For each sampled pMSSM point, the Superiso 4.1 package [37] is used to calculate the values of nine additional B-physics observables from the spectrum provided by SPheno. Superiso also provides the compatibility of the calculated observables with existing measurements in the form of a χ^2, which is incorporated into the likelihood according to

$$L = \frac{(\chi^2)^{(\frac{n}{2}-1)}}{2^{\frac{n}{2}}\Gamma(\frac{n}{2})} e^{-\chi^2/2} \,, \tag{1}$$

where n is the number of measurements. The B-physics observables included in the Superiso χ^2 are listed in Table 3, corresponding to $n = 9$.

Observable	**N(meas.)**
$\Delta_0(B \to K\gamma)$	1
$BR(B^0 \to K^{*0}\gamma)$	1
$BR(B_s \to \mu\mu)$	1
$BR(B_d \to \mu\mu)$	1
$BR(b \to s\gamma)$	1
$BR(b \to s\mu\mu)$	2
$BR(b \to see)$	2

Table 3: B-physics observables included in the calculation the χ^2 from Superiso. For the last two rows, measurements from two energy regions are included.

HiggsSignals 2.6.0 [38, 39] is then used to calculate each point's compatibility with LHC Higgs rate measurements, including measurements of the Higgs boson mass. HiggsSignals returns a χ^2 value, which is incorporated into the total likelihood according to Equation 1 with number of degrees of freedom $n = 107$. The likelihood corresponding to $H/A \to \tau\tau$ searches at the LHC is calculated by HiggsBounds 5.9.1 [40–44] and included in the total McMC likelihood (for the application of the other search channels, see below).

The difference between the standard model value and the pMSSM value for the anomalous muon magnetic moment, Δa_μ, is calculated for each point by the GM2Calc package [45, 46]. In order to allow for sufficient statistics near both the SM value of $\Delta a_\mu = 0$ and the measured central value of $\Delta a_\mu = 251 \times 10^{-11}$ [47], Δa_μ is included in the likelihood for only half of the scan threads. When included in the likelihood, the Δa_μ contribution is taken to be Gaussian with mean corresponding to the measured central value, with the same value (251×10^{-11}) used for the width. This approach ensures that pMSSM regions near the measured value and the SM prediction are both populated by the scan.

The McMC likelihood does not include the following observables, though their values are computed for each point to allow understanding of how the allowed pMSSM space relates to physical observables of interest:

- Character and composition of the lightest neutralino, which is taken as the DM candidate;
- DM-nucleon cross sections;
- DM relic density Ωh^2.

2.2 Stepping in the McMC

Given pMSSM point $\vec{x}$, the stepping functions $f_i(x_i)$ are the probability distributions from which the next pMSSM point is chosen, where i is the parameter index. Two forms are considered for the stepping functions in the pMSSM scan. The first is denoted **linear**:

$$f(x_i) = \text{Gaus}(\mu = x_i, \sigma = \sigma_0 \times w) \,. \tag{2}$$

Here, w is the width of the parameter range allowed for parameter x_i (see Table 1), and σ_0 is a tunable step size parameter. The second stepping function is denoted **logarithmic**:

$$f(x_i) = \exp\left[\text{Gaus}(\mu = \ln|x_i|, \sigma = \sigma_0 \times w)\right] \,, \tag{3}$$

where w and σ_0 have the same meanings as above.

Because the logarithmic stepping function is positive definite, each new point selected from this distribution will have positive sign. However, some pMSSM parameters can have negative values (M_1, M_2, μ, A_t, A_b, A_l). The sign of each parameter is therefore fixed to that of the randomly selected initial point, and the magnitude only is determined by the stepping function. The final combination of many scans with different initial points ensures that all sign combinations are explored.

Relative to the linear stepping function, the logarithmic stepping function ensures that lower parameter values are explored with finer granularity than higher ones. This has several advantages for the pMSSM scan. First, the highest parameter values are inaccessible to many collider scenarios of interest for Snowmass 2021, and the use of log stepping in some or all parameters ensures that the scan is not overwhelmed by points only accessible at a 100 TeV proton-proton collider. Second, at lower sparticle masses, it becomes more likely to obtain so called "compressed spectra" in which a more diverse array of experimental signatures result from small differences between sparticle masses.

A series of small-scale (200,000 point) test scans are generated to optimize the choice of stepping functions. In these tests, the logarithmic stepping function is taken as the default for all pMSSM parameters, and four values of the step size are tested: $\sigma_0 = 0.05$, 0.10, 0.20, and 0.30. These scans are labelled by "Log σ_0" for the remainder of this section. An additional scan setup, "Lin 0.05", aims to sample a higher fraction of points where the strong SUSY sector is decoupled: here, the logarithmic stepping function ($\sigma_0 = 0.05$) is used for all but the squark and gluino mass parameters, which instead employ the linear stepping function with $\sigma_0 = 0.05$.

Figure 1 shows the distribution of gluino (top) up-type squark (bottom) mass parameters for points sampled by the McMC for the different stepping configurations. For the logarithmic stepping scenarios, an increase in σ_0 corresponds to an increase in the slope of the distribution, and therefore to the fraction of events with high squark masses.

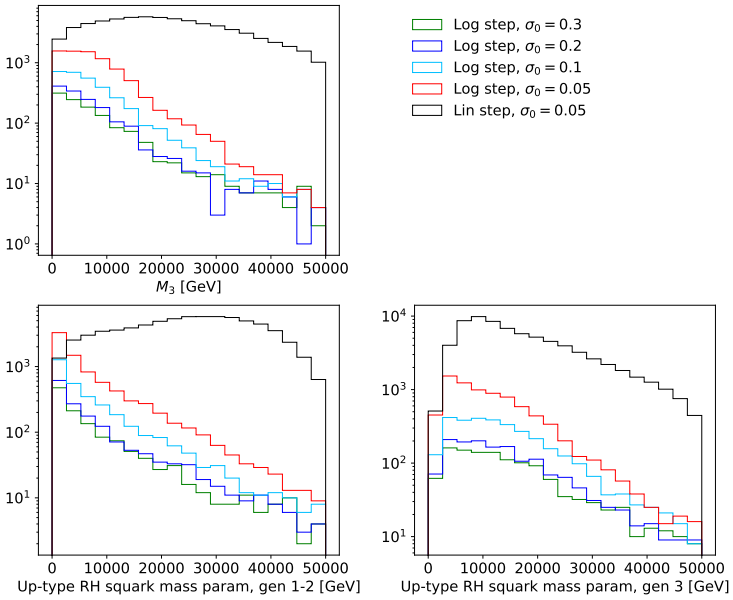

Figure 1: Squark and gluino mass parameter values of sampled pMSSM points accepted by the McMC, shown for different stepping configurations. The black distribution corresponds to Lin 0.05, which is chosen as the baseline.

The test scan setups are listed in the top section of Table 4. The middle section of this table reports the number of points sampled, accepted by the McMC, and accepted after post-processing (described in Section

3), as well as the total efficiency.

The lower portion of Table 4 shows the fraction of points in a few regions that are of special interest:

- Strong SUSY sector is decoupled: lightest squark or gluino mass > 10 TeV;
- Compressed mass spectra: Δm between the lightest SUSY particle (LSP) and the stop or gluino < 500 GeV.

A high density of points in both regions is useful for Snowmass 2021 studies.

	Log 0.05	Log 0.10	Log 0.20	Log 0.30	Lin 0.05
Stepping ($\tilde{q}$, $\tilde{g}$)	log	log	log	log	lin
Stepping (other)	log	log	log	log	log
Step width σ_0	5%	10%	20%	30%	5%
Sampled points	200,100	200,100	200,100	200,100	200,100
McMC accepted points	1,376	483	227	178	46,141
Post-process accepted points	345	124	53	46	23,064
Total Efficiency	0.17%	0.06%	0.03%	0.02%	11.8%
Strong decoupling	34	22	18	13	3,917
$\Delta m(\text{LSP} - \tilde{g}) < 500$ GeV	4	2	0	0	13
$\Delta m(\text{LSP} - \tilde{t}) < 500$ GeV	2	0	0	0	9

Table 4: Results of the test scans with different stepping configurations. The criteria for points with strong decoupling is that the squark, gluino masses are all > 10 TeV.

The Lin 0.05 setup contains the highest fraction of points with squark and gluino masses above 10 TeV, as seen in both Figure 1 and Table 4. Largely for this reason, the Lin 0.05 test scan is deemed the most optimal and is used as the final stepping configuration.

In order to maximize the statistics of the final scan, the results of the four non-optimal test scans presented in this section are combined with the results of the final configuration. However, the contribution from these test scans is small, and the overall scan behavior follows that of Lin 0.05.

3 Selection of sampled points

Following the sampling of pMSSM points, a post-processing step is applied to further remove experimentally disfavored regions of the parameter space from the scan. In particular, points are rejected if they satisfy one or more of the following criteria:

- excluded at 95% CL by LHC Higgs searches, as calculated by HiggsBounds;
- excluded at 95% CL by LHC SUSY searches, as calculated by SModelS [48–51];
- excluded at 95% CL by dark matter measurements, as calculated by MicrOMEGAs [52–54].

The HiggsBounds likelihood of the $H/A \to \tau\tau$ search is used directly in the McMC likelihood described above. However, the boolean constraints calculated by HiggsBounds, which indicate whether a point is excluded by LHC Higgs searches, are applied only at the post-processing stage. HiggsBounds tests each of the Higgs bosons individually, where in each case the potentially strongest bound (i.e. the channel with the highest expected sensitivity) is applied. A pMSSM point is rejected if it is excluded at 95% CL by at least one of the applied Higgs boson search channels.

The exclusion limits from LHC SMS searches on each pMSSM point are calculated by SModelS 2.1 [48–51]. SModelS first decomposes each pMSSM point into all relevant SMS models, then computest the cross section of the simplified model processes. Finally, the cross section of each simplified model process is compared to to the experimental limit. The pMSSM point is rejected if any simplified model process is excluded at 95% CL.

The MicrOMEGAs package [52] 5.2.7.a calculates exclusion limits from $Z \rightarrow$ invisible, DM direct detection experiments [54], and searches for sparticle and DM production in e^+e^- collisions from LEP [53]. Points excluded by any of these measurements at 90% CL are rejected. The DM relic density Ωh^2 is also calculated at the post-processing step by MicrOMEGAs. Though not included in the McMC likelihood, this observable can be used to further focus on regions of the pMSSM scan that are experimentally and theoretically motivated.

An overview of the scanned pMSSM points is shown in Table 5. The first and second columns show the portions of the scan that do and do not use Δa_μ in the McMC likelihood, respectively. Note that the scan efficiency is much higher when Δa_μ is not included in the likelihood, but the fraction of points with Δa_μ near the measured value (last row) is small. The total scan statistics, corresponding to the sum of the first two columns, are shown in the final column of Table 5.

	With Δa_μ	Without Δa_μ	Total
Sampled points	14,194,316	16,848,695	31,043,011
McMC accepted points	156,599	6,800,642	6,957,241
Post-process accepted points	44,444	3,312,480	3,356,924
Total Efficiency 0.3%	20%	11%	
Strong decoupling	5,529	577,695	583,224
Δm(LSP, gluino) < 500 GeV	24	2,412	2,436
Δm(LSP, stop) < 500 GeV	14	1,480	1,494
Δa_μ within measured $\pm 1\sigma$ of	19,540	3,212	22,752

Table 5: Summary of the scanned pMSSM points. The criteria for points with strong decoupling is that the squark, gluino masses are all > 10 TeV.

4 Results

Precision measurements of sensitive observables can be a powerful tool for constraining physics beyond the standard model. This section presents studies of a select few observables, and how future experiments are projected to impact the allowed pMSSM space.

4.1 Higgs boson properties

Higgs boson couplings for each pMSSM point are calculated by FeynHiggs and studied in the κ-framework [55, 56], where for particle p with Higgs coupling λ_p

$$\kappa_p = \frac{\lambda_p}{\lambda_{p,\mathrm{SM}}} \ . \tag{4}$$

The Higgs boson coupling to quarks (top, bottom, and charm) and leptons (tau and muon) are found to peak sharply the expected SM value of $\kappa = 1$. This is consistent with the LHC measurements to date, which enter the McMC likelihood through the contribution from HiggsSignals.

The couplings to the top quark, bottom quark, and tau lepton are shown for each pMSSM point in Figure 2. The sampled pMSSM points that are excluded at post-processing are shown separately from the final accepted sample. Points accepted by the McMC but excluded at 95% CL by HiggsBounds (LHC Higgs searches) are shown in purple. Of the remaining points, those excluded at 95% CL by SModelS (LHC SUSY searches) are shown in dark blue. And of the remaining points, those excluded at 95% CL by MicrOMEGAs (DM measurements) are shown in light blue. The green distribution shows the points that are fully accepted after all post-processing steps.

The distributions of κ_c and κ_μ (not shown) closely resemble those of κ_t and κ_τ, respectively. The distributions found for κ_t, κ_b and κ_τ, as shown in Figure 2, agree with the deviations expected in a 2HDM type II, i.e. the tree-level structure of the MSSM Higgs sector.[1] The deviations from unity scale with

[1] Genuine SUSY contributions to the various Higgs-boson couplings have been found to be relatively small [57].

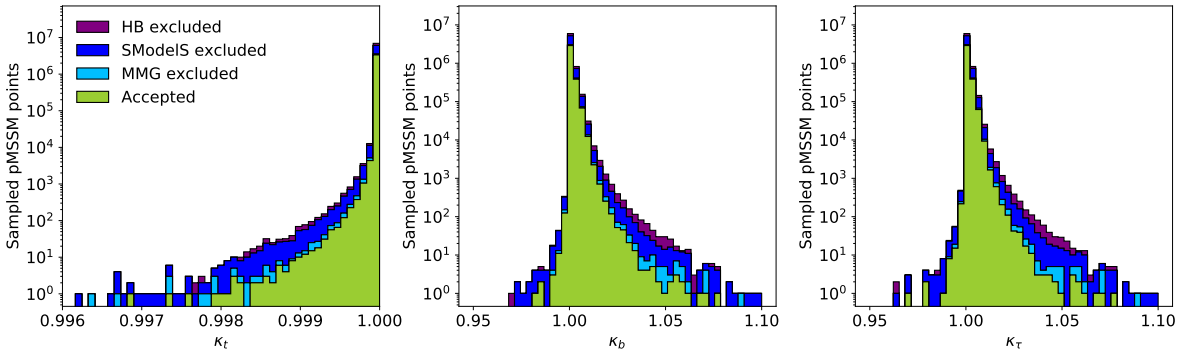

Figure 2: Higgs couplings κ_t, κ_b, and κ_τ calculated by FeynHiggs for each pMSSM point.

$\sin(\beta-\alpha)+\cos(\beta-\alpha)/\tan\beta$ for κ_t and with $\sin(\beta-\alpha)-\cos(\beta-\alpha)\tan\beta$ for $\kappa_{b,\tau}$ (α is the angle that diagonalizes the CP-even Higgs sector). For $M_A \to \infty$ one finds $\beta-\alpha \to \pi/2$ ($\sin(\beta-\alpha) \to 1$). Consequently, for $\tan\beta > 1$ (as in this scan) one finds smaller deviations from unity for κ_t and larger opposite sign deviations for $\kappa_{b,\tau}$. The pseudo-scalar component of each Higgs-fermion coupling is also calculated, but is not found to deviate from zero in any of the sampled pMSSM points. Taking into account the size of the deviations of $\kappa_{t,b,\tau}$ from unity and the expected experimental precision at current and future experiments in the various κ determinations, κ_b is clearly the quantity to search for deviations from the SM.

Three benchmarks [58] are selected to quantify future precision on the Higgs-bottom quark coupling κ_b:

- the projected precision of ILC 250: $\kappa_b = 1 \pm 1.8\%$;
- the projected precision of FCC ee 240: $\kappa_b = 1 \pm 1.3\%$;
- the projected precision of FCC ee/eh/hh: $\kappa_b = 1 \pm 0.43\%$;

The fraction of sampled pMSSM points with κ_b within $\pm 1\sigma$ of the SM value is shown in Figure 3 as a function of M_A (left) and $\tan\beta$ (right). The ILC, FCC ee, and FCC ee/eh/hh benchmarks are shown in black, orange, and red, respectively. Increasing the anticipated precision on κ_b cuts away particularly points at low M_A as observed in the left plot, in agreement with the expected decoupling behavior. The behavior with $\tan\beta$ shows that for fixed M_A the decoupling approached for increasing $\tan\beta$.

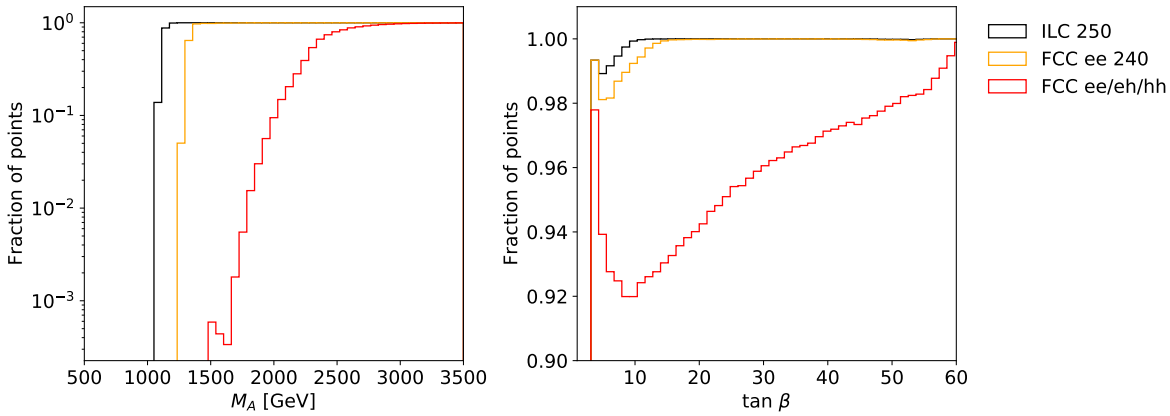

Figure 3: Fraction of scanned pMSSM points with κ_b within $\pm 1\sigma$ of the SM value, as a function of M_A (left) and $\tan\beta$ (right). The ILC, FCC ee, and FCC ee/eh/hh 1σ benchmarks are shown in black, orange, and red, respectively.

Figure 4 shows the fraction of the sampled pMSSM points in the M_A–$\tan\beta$ plane that are found with κ_b close to unity within $\pm 1\%$ (corresponding roughly to the anticiated 95% CL FCC ee/eh/hh limit) in the

left and within ±0.2% in the right plot. The gray region is excluded by current searches for heavy MSSM Higgs bosons. The 1% limit cuts away most points below $M_A \leq 2000$ GeV, setting an indirect lower bound on the MSSM heavy Higgs mass scale. A stronger bound can be found for the increased precision of 0.2%, where $M_A \sim 2$ TeV would only be allowed for large $\tan\beta$ values. The projected limits from direct searches for heavy MSSM Higgs bosons at the HL-LHC (cyan) and the FCC-hh (green) are overlaid. Even with the full precision on κ_b expected at the FCC-hh, the indirect limit is far less powerful than direct searches.

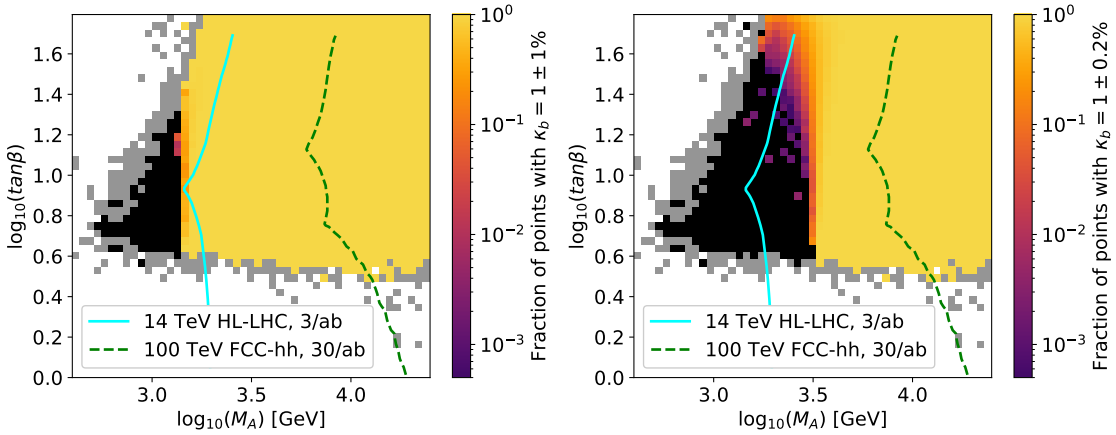

Figure 4: Fraction sampled pMSSM points with κ_b within ±1% (left) and ±0.2% (right) of the SM expectation, shown as a function of $\tan\beta$ and M_A. The projected limits from direct searches for heavy MSSM Higgs bosons at the HL-LHC (cyan) and the FCC-hh (green) are overlaid.

The effective coupling of the Higgs boson to photons, which occurs through loop processes dominated by the W boson and top quark, is another sensitive observable due to the high experimental precision achievable in diphoton final states. This effective coupling, κ_γ, is defined by

$$\kappa_\gamma^2 = \frac{\mathrm{BR}(H \to \gamma\gamma)}{\mathrm{BR}_{\mathrm{SM}}(H \to \gamma\gamma)}. \tag{5}$$

The distribution of κ_γ for the sampled pMSSM points is shown in Figure 5. Values of $\kappa_\gamma > 1.25$ are excluded by existing Higgs measurements.

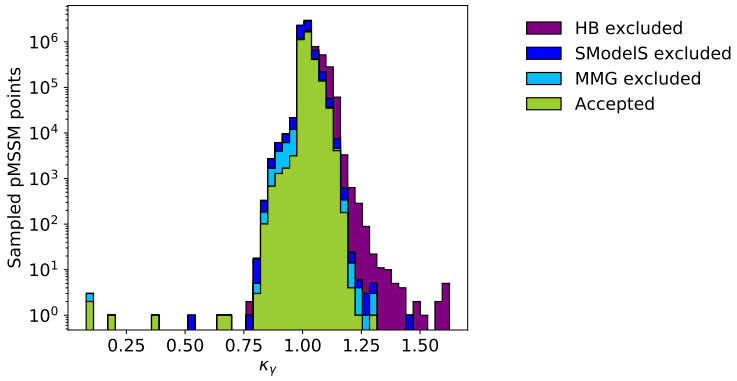

Figure 5: Effective Higgs-photon coupling, κ_γ, calculated by FeynHiggs for each pMSSM point.

Figure 6 shows the fraction of the sampled pMSSM points in the M_A–$\tan\beta$ plane that are found with κ_γ close to unity within ±0.6% (corresponding roughly to the anticiated 95% CL FCC ee/eh/hh limit) in the left and within ±0.1% in the right plot. As in Figure 4, the gray region is excluded by current searches for

heavy MSSM Higgs bosons. As precision on κ_γ increases, points with low $\tan\beta$ are cut away because Sven knows!.

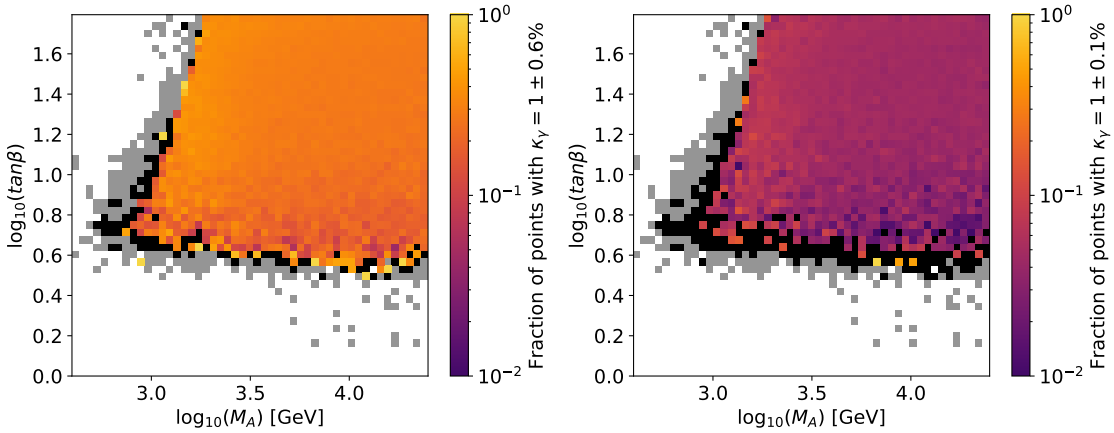

Figure 6: Fraction sampled pMSSM points with κ_γ within $\pm 0.6\%$ (left) and $\pm 0.1\%$ (right) of the SM expectation, shown as a function of $\tan\beta$ and M_A.

Similarly, figure 7 shows the fraction of points in the chargino-neutralino mass plane with κ_γ within $1 \pm 0.6\%$ (left) and $1 \pm 0.1\%$ (right). The gray regions are excluded by existing measurements: the low chargino mass region by mass limits from LEP and $Z \to$ invisible, and the other blob XXXX. With increasing precision on κ_γ, model points with light charginos are excluded because Sven knows!.

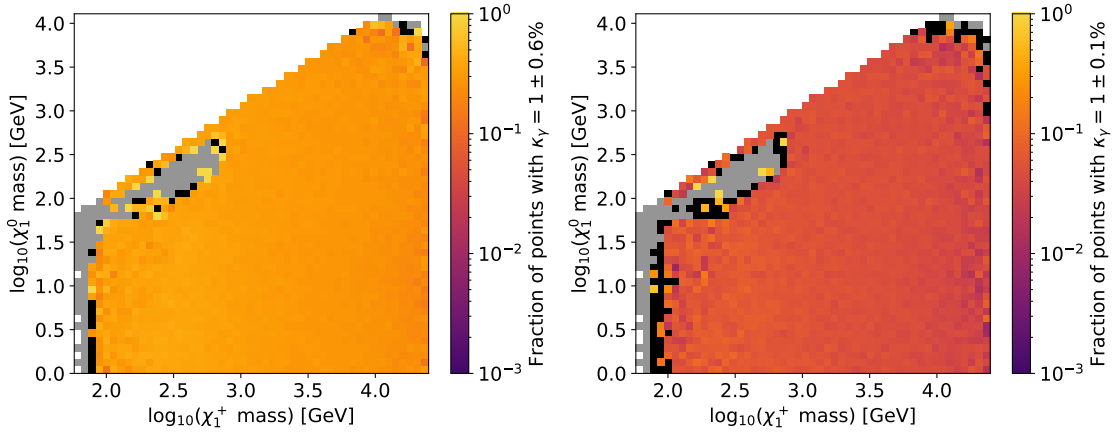

Figure 7: Fraction sampled pMSSM points with $\kappa\gamma$ within $\pm 0.6\%$ (left) and $\pm 0.1\%$ (right) of the SM expectation, shown as a function of chargino and neutralino masses.

4.2 Anomalous magnetic moment of the muon

Recent measurements of the anomalous muon magnetic moment Δa_μ [47] in comparison with the SM prediction [59] have sparked renewed interest in possible physics beyond the SM contributing to this observable. The McMC likelihood is therefore constructed to populate the region near the measured value as well as the value predicted within the SM ($\Delta a_\mu = 0$). The distribution of Δa_μ for the sampled pMSSM points, shown in Figure 8, exhibits the desired two-peak structure. Though much of the peak at the measured value is excluded by SModelS, approximately 10% of points passing all selection have Δa_μ within 1σ of the measurement (denoted by vertical lines).

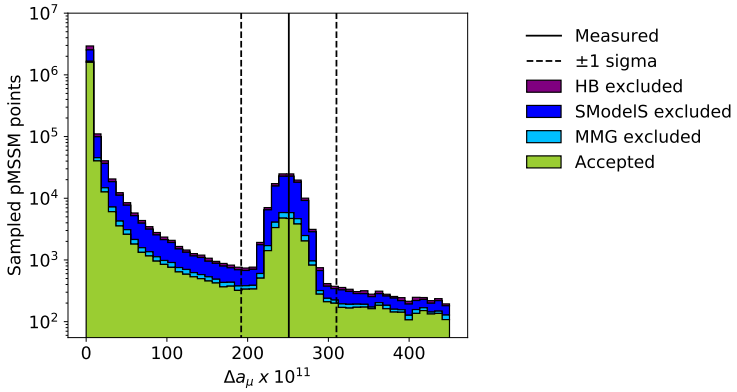

Figure 8: Distribution of Δa_μ for the sampled pMSSM points. The predicted Standard Model value corresponds to $\Delta a_\mu = 0$, and the measured central value and uncertainties indicated by vertical lines.

In order to achieve a value of Δa_μ near the measured value of $\Delta a_\mu = 251 \times 10^{-11}$, SUSY contributions involving smuon-neutralino or muon sneutrino-chargino loops are required. The corresponding particle masses should not be too high, not to suppress these loop contributions, leading typically to a light smuon (see, e.g., [60]). The fraction of sampled pMSSM points with Δa_μ within $\pm 1\sigma$ of the measured value is shown in Figure 9 as a function of the smuon mass. Three values of σ are considered: the uncertainty on the 2021 Muon $g-2$ measurement (59×10^{-11}), the projected uncertainty at the end of running of the Muon $g-2$ experiment (a factor of two improvement in over 2021 in the combined experimental and theoretical uncertainty), and a potential future precision benchmark of five times higher precision than the 2021 result. The fraction of sampled points satisfying the $\pm 1\sigma$ criterion is high for low values of the smuon mass (< 3 TeV).

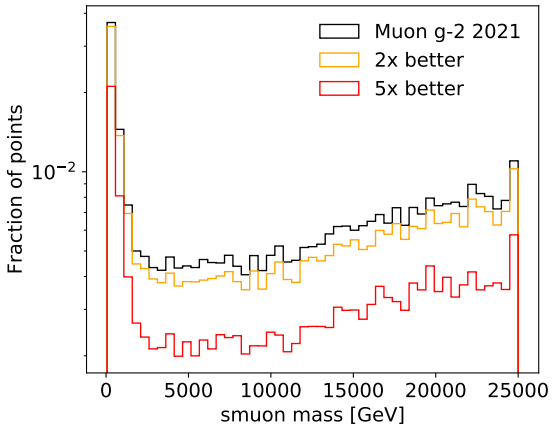

Figure 9: Fraction of scanned pMSSM points with Δa_μ within $\pm 1\sigma$ of the measured value, as a function of the smuon mass. The black line corresponds to the measured 2021 uncertainty $\sigma = 59 \times 10^{-11}$. The green and red lines correspond to a reduction in σ of a factor of two and five, respectively.

4.3 Electroweakino dark matter

The DM particle is taken to correspond to the lightest neutralino in the model, $\tilde{\chi}_1^0$. The DM relic density, Ωh^2, is calculated by MicrOMEGAs. Figure 10 shows the relic density of the scanned pMSSM points, with the Planck measurement [61] indicated by a vertical line. The pMSSM scan populates values of this parameter over a very wide range compared to the experimental precision. The impact of LHC searches on the allowed values of Ωh^2 is quite pronounced: the majority of points with low relic density are excluded by SModelS.

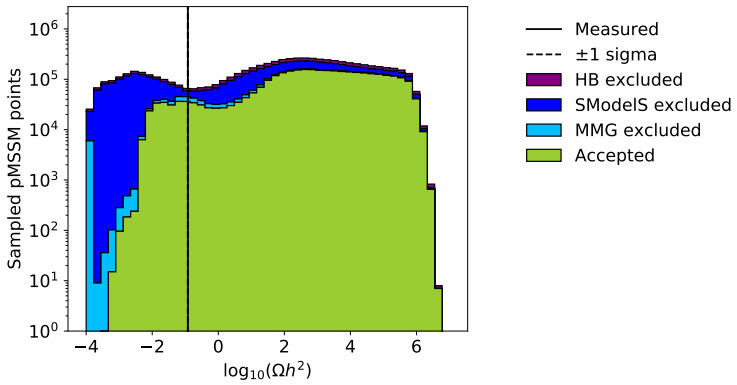

Figure 10: The DM relic density for each sampled pMSSM point. The measured value of Ωh^2 is indicated by vertical lines.

The DM candidate particle is a superposition of electroweakino states (bino, wino[2], and higgsino). Each pMSSM point is labelled by the electroweakino comprising the largest component of χ_1^0, thereby separating the scan into samples with bino-, wino-, and higgsino-like DM. Table 6 shows the breakdown of pMSSM points by the composition of the DM candidate.

	McMC accepted	Post-process accepted
Mostly wino	872,256	188,576
Mostly bino	5,513,680	3,071,103
Mostly higgsino	506,469	97,222
Mixed wino/bino	172	6
Mixed bino/higgsino	9,219	2
Mixed wino/higgsino	8,100	1
Other	47,445	14

Table 6: Number of scanned pMSSM points with different composition of the DM candidate. The DM candidate is considered mostly pure if a single electroweakino comprises $> 80\%$ of the admixture, and mixed if two components each contribute $> 40\%$.

The DM relic density for each component sample is shown in Figure 11. The sampled points with very high relic density are dominated by models with bino-like DM. Wino-like DM, on the other hand, is concentrated at low values of Ωh^2. Near the measured value of the relic density, wino-, bino-, and higgsino-like DM all contribute.

The two dimensional distribution in the space of the relic density and DM particle mass is shown in Figure 12. Points that are excluded by SModelS, HiggsBounds, and MicrOMEGAS are shown in light gray, and accepted points are color-coded by the DM composition. The Z- and Higgs-funnels, where the bosons contribute resonantly to the DM annihilation cross section, are clearly visible. Points in these funnel regions with relic density less than ~ 0.1 are excluded by DM direct detection and mass limits from LEP. The region near neutralion mass $\sim$ 100 GeV and $\Omega h^2 \sim 0.01$ is excluded by SMS searches at the LHC, particularly XXXXXXXX. Points with neutralino mass less than $\sim$ 1 GeV are excluded at lower relic density by limits from $Z \rightarrow$ invisible.

Figure 13 shows the two dimensional distribution of the DM candidate mass and DM-neutron spin-independent cross section. The cross DM-proton spin-independent cross section gives a similar distribution. As in Figure 12, points that are excluded by SModelS, HiggsBounds, and MicrOMEGAS are shown in light gray, and accepted points are color-coded by the DM composition. The exclusion due to DM direct detection

[2]Keep in mind that the on-shell mass spectrum in the chargino/neutralino sector in the case of wino DM requires higher-order corrections that depend on the hierarchy of M_2, M_1 and μ. These corrections so far cannot be taken into account in automated way (see the discussion in [62]). Consequently, the results shown here for wino DM cannot be regarded as fully reliable.

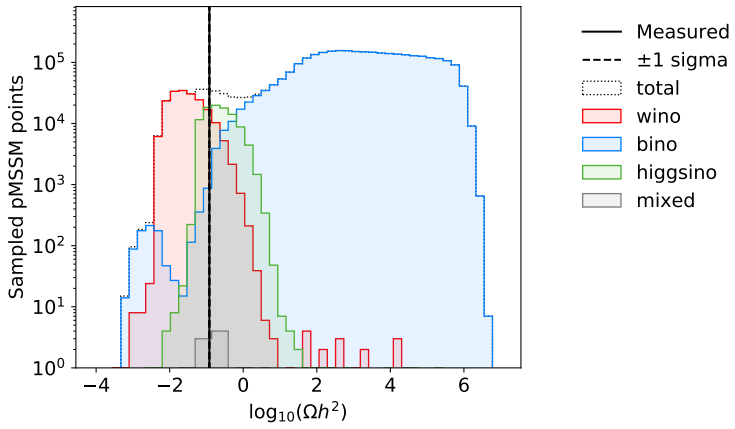

Figure 11: Distribution of the dark matter relic density for the sampled pMSSM points, after the full selection has been applied, broken down by the electroweakino composition of the dark matter candidate.

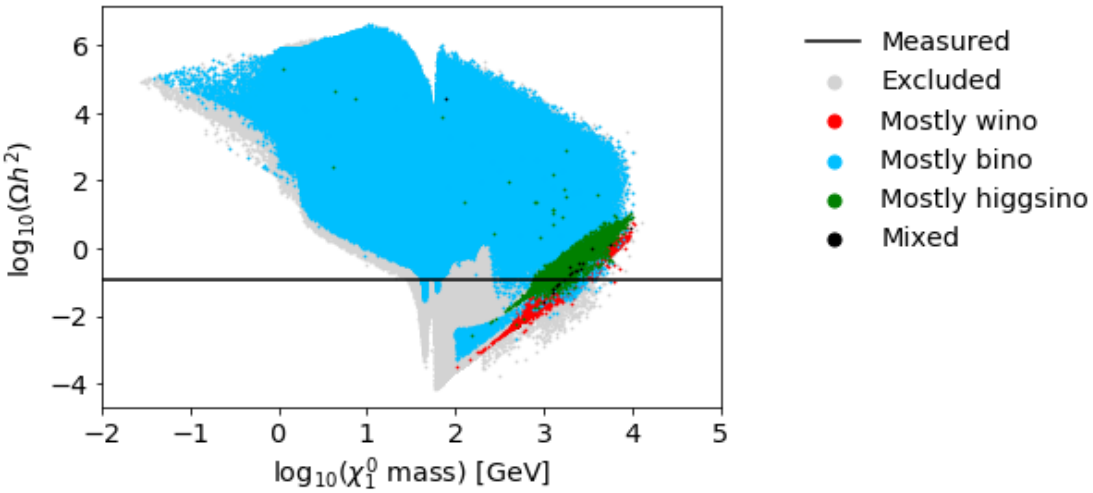

Figure 12: Distribution of the DM candidate mass and relic density for the sampled pMSSM points. Points excluded by existing measurements are shown in light gray. The remaining points are broken down by the electroweakino composition of the DM candidate. The DM candidate is considered mostly pure if a single electroweakino comprises $> 80\%$ of the admixture, and mixed otherwise.

experiments is clearly visible at high cross section values in the region above $m(\chi_1^0) \sim 10$ GeV. Additional exclusions from LHC SMS searches for heavy stable charged particles [**XXXX**] contribute to the dip in allowed cross section in the range 100-1000 GeV.

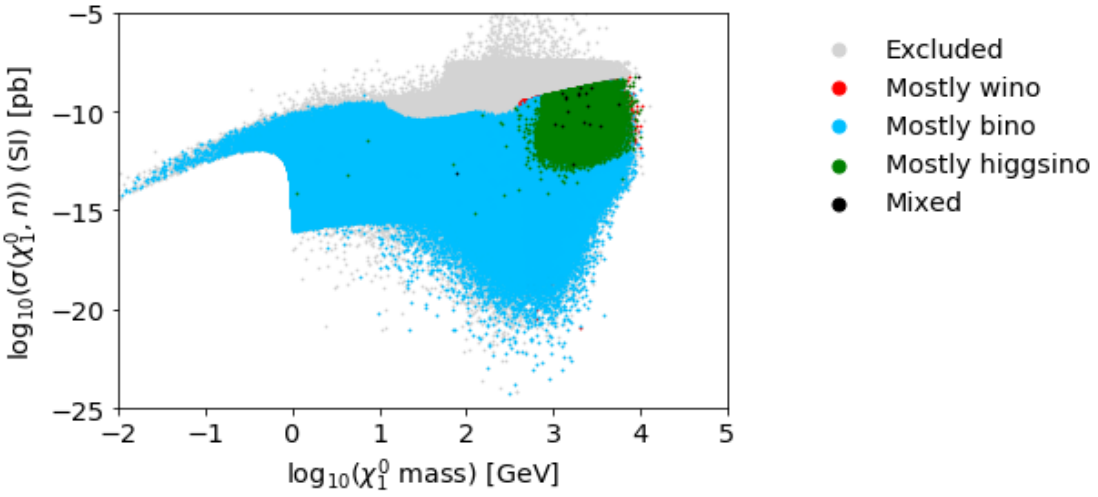

Figure 13: Distribution of the DM candidate mass and DM-neutron spin-independent cross section for the sampled pMSSM points. Points excluded by existing measurements are shown in light gray. The remaining points are broken down by the electroweakino composition of the DM candidate.

5 Summarizing the kinematics of non-excluded pMSSM models

Models resulting from a pMSSM scan and that have not been excluded by experimental results can be used to identify new promising regions in experimental observable space (the space made up of all experimental observables, such as momenta of particles and invariant masses of combinations of particles) which can be studied to develop future BSM searches and even guide future experimental design. Non-excluded models were explored in previous ATLAS and CMS searches WH: not sure if I should cite the ATLAS and CMS results again to understand why they evaded the reach of these experiments. Within ATLAS, some of these models had their mass spectra manually inspected to gain insight into their expected signature in experimental observable space. However, the experimental observable space of the non-excluded models was not systematically probed and no new searches were designed on the basis of the non-excluded models, owing to the difficulty of interpreting thousands of models manually. CMS interpreted the non-excluded models as a function of average values of observables. This yielded valuable information about the observables of non-excluded models, but was difficult to interpret because of the large number of models.

Systematically probing the observable space of non-excluded models requires novel techniques that are able to summarize thousands of models that populate high-dimensional observable spaces. Machine learning (ML) is especially adept at processing high-dimensional spaces and can be utilized to identify promising new search regions inspired by the pMSSM. In particular, ML clustering techniques, which group similar data points together, could group multiple models with different theory parameters but similar experimental signatures, forming the basis for new search regions (since the regions are based on models that have evaded previous searches). A sketch of the proposed clustering workflow is shown in Figure 14. Once a set of regions has been selected, further studies can be performed to assess the viability of robustly estimating SM backgrounds for these regions with (semi)-data-driven methods. (These studies would address questions such as the following: Can a control region with sufficient data statistics be designed?)

Several techniques, such as k-means [63] and density-based clustering [64], exist that can be used to group models with similar experimental signatures together. Feasibility studies were performed which were based on SMS searches for new physics in events with two top quarks and significant missing transverse energy in the all-hadronic channel. The simplified model has two parameters, the top squark mass ($m_{\tilde{t}}$) and the

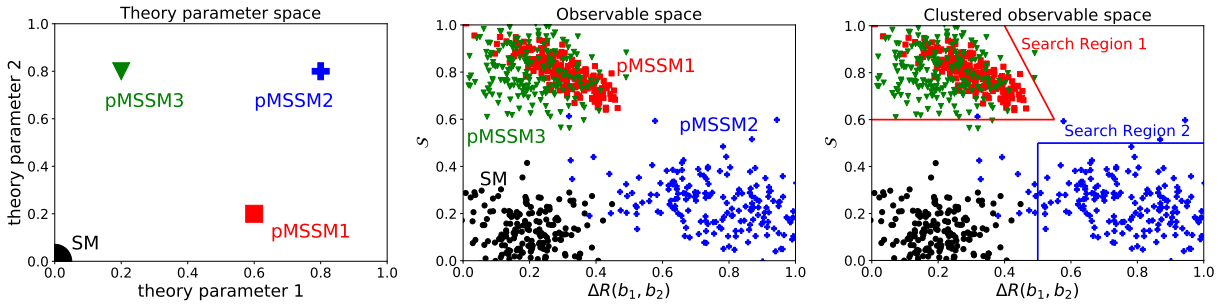

(a) Theory parameter space (b) Observable space (c) Clustering-produced regions

Figure 14: Workflow for interpreting non-excluded pMSSM models with clustering in a toy example two-dimensional space. The two theory parameter values for four models (SM, pMSSM1-3) are shown in (a), while the space that these models populate in experimental observable space (filled with MC simulations of the models) is shown in (b) and (c).

neutralino mass ($m_{\tilde{\chi}^0}$), which have a known effect on the observable space. A five-dimensional observable space, consisting of common variables used in analyses (i.e., MET, HT, p_T's of the leading four jets, and jet multiplicity), was clustered using the k-means+gap statistic [65] method. Additionally, simulations of a grid of SMS models with different theory parameter values, expected to be associated with distinct distributions of their observables, were produces using Madgraph+Delphes. The results of applying k-means to form clusters of this theory model grid in the two-dimensional theory parameter space are shown in Figure 15a and demonstrate that k-means groups models in a similar way as the manually designed search (which had three major regions [66]). The exact number of clusters (i.e., regions) is not important, since the final goal of the approach is to reduce thousands of models to a handful of promising regions. Similar to the visualization used in the Run 1 CMS pMSSM scan, Figure 15b shows the median and 68% confidence interval (CI) of the observables used for clustering for each of the clusters. Figure 15b could have included all the SMS models but this would have been more difficult to interpret and would yield less insight into what type of regions could be designed to be sensitive to non-excluded models. The reduction from 100s of SMS models to three regions significantly helps the interpretability of the kinematics of the non-excluded models. Figure 15b also shows

Applying the above clustering technique to pMSSM scans which include future experiments and colliders could guide detector and trigger design by identifying regions of observable space that are populated by pMSSM models but for which a proposed analysis, trigger, or detector designs have limited sensitivity.

6 Conclusion

An extensive scan of the pMSSM parameter space has been completed for Snowmass 2021. The scanned parameter space covers ranges that will be accessible ranges to many future collider scenarios, including electron, muon, and hadron colliders at a center of mass energies up to 100 TeV. The choice of a Markov chain Monte Carlo sampling method ensures that the 19 dimensional parameter space is explored efficiently. The inclusion of current measurements in the likelihood ensures that space that is experimentally disfavored is not prioritized. Additional selection at the post-processing stage accounts for the effects of LHC Higgs and SUSY SMS searches and DM measurements. The impact of future precision measurements on Higgs couplings, Δa_μ, and DM quantities is presented.

Future plans. Jim

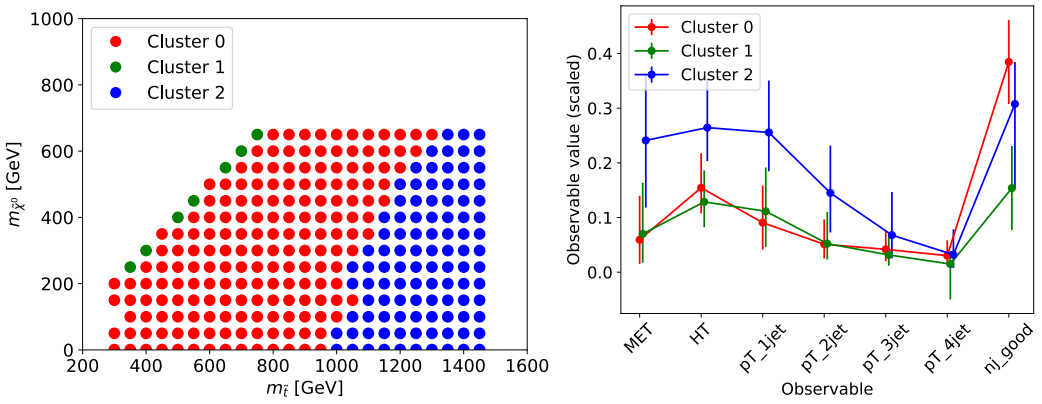

(a) (b)

Figure 15: Division of a SMS model grid (a) after applying k-means on common observables. The median and 68% CI bands of observables are shown in (b) which indicates that the leading difference for these models is the MET and jet multiplicity, as expected. The green dots correspond to a region where the sparticle masses are similar and thus only low- objects are produced which results in a low jet multiplicity. The red dots, on the other hand, are have large sparticle mass splittings which results in large MET. The y-axis of (b) is the value of the observable after being normalized to be in a range of [0,1].

References

[1] P. Fayet. "Supersymmetry and weak, electromagnetic and strong interactions". In: *Physics Letters B* 64.2 (1976), pp. 159–162. ISSN: 0370-2693. DOI: https://doi.org/10.1016/0370-2693(76)90319-1. URL: https://www.sciencedirect.com/science/article/pii/0370269376903191.

[2] P. Fayet. "Spontaneously broken supersymmetric theories of weak, electromagnetic and strong interactions". In: *Physics Letters B* 69.4 (1977), pp. 489–494. ISSN: 0370-2693. DOI: https://doi.org/10.1016/0370-2693(77)90852-8. URL: https://www.sciencedirect.com/science/article/pii/0370269377908528.

[3] Glennys R. Farrar and Pierre Fayet. "Phenomenology of the production, decay, and detection of new hadronic states associated with supersymmetry". In: *Physics Letters B* 76.5 (1978), pp. 575–579. ISSN: 0370-2693. DOI: https://doi.org/10.1016/0370-2693(78)90858-4. URL: https://www.sciencedirect.com/science/article/pii/0370269378908584.

[4] Pierre Fayet. "Relations between the masses of the superpartners of leptons and quarks, the goldstino coupling and the neutral currents". In: *Physics Letters B* 84.4 (1979), pp. 416–420. ISSN: 0370-2693. DOI: https://doi.org/10.1016/0370-2693(79)91229-2. URL: https://www.sciencedirect.com/science/article/pii/0370269379912292.

[5] Savas Dimopoulos and Howard Georgi. "Softly broken supersymmetry and SU(5)". In: *Nuclear Physics B* 193.1 (1981), pp. 150–162. ISSN: 0550-3213. DOI: https://doi.org/10.1016/0550-3213(81)90522-8. URL: https://www.sciencedirect.com/science/article/pii/0550321381905228.

[6] Ali H. Chamseddine, Richard L. Arnowitt, and Pran Nath. "Locally Supersymmetric Grand Unification". In: *Phys. Rev. Lett.* 49 (1982), p. 970. DOI: 10.1103/PhysRevLett.49.970.

[7] Riccardo Barbieri, S. Ferrara, and Carlos A. Savoy. "Gauge Models with Spontaneously Broken Local Supersymmetry". In: *Phys. Lett. B* 119 (1982), p. 343. DOI: 10.1016/0370-2693(82)90685-2.

[8] Luis E. Ibanez. "Locally Supersymmetric SU(5) Grand Unification". In: *Phys. Lett. B* 118 (1982), pp. 73–78. DOI: 10.1016/0370-2693(82)90604-9.

[9] Lawrence J. Hall, Joseph D. Lykken, and Steven Weinberg. "Supergravity as the Messenger of Supersymmetry Breaking". In: *Phys. Rev. D* 27 (1983), pp. 2359–2378. DOI: 10.1103/PhysRevD.27.2359.

[10] Johan Alwall, Philip C. Schuster, and Natalia Toro. "Simplified models for a first characterization of new physics at the LHC". In: *Physical Review D* 79.7 (Apr. 2009). ISSN: 1550-2368. DOI: 10.1103/physrevd.79.075020. URL: http://dx.doi.org/10.1103/PhysRevD.79.075020.

[11] Daniele Alves et al. "Simplified models for LHC new physics searches". In: *Journal of Physics G: Nuclear and Particle Physics* 39.10 (Sept. 2012), p. 105005. ISSN: 1361-6471. DOI: 10.1088/0954-3899/39/10/105005. URL: http://dx.doi.org/10.1088/0954-3899/39/10/105005.

[12] S. Chatrchyan et al. "Interpretation of searches for supersymmetry with simplified models". In: *Physical Review D* 88.5 (Sept. 2013). ISSN: 1550-2368. DOI: 10.1103/physrevd.88.052017. URL: http://dx.doi.org/10.1103/PhysRevD.88.052017.

[13] ATLAS Collaboration. "Summary of the ATLAS experiment's sensitivity to supersymmetry after LHC Run 1 — interpreted in the phenomenological MSSM". In: *JHEP* 2015.10 (Oct. 2015). DOI: 10.1007/jhep10(2015)134. arXiv: 1508.06608 [hep-ex].

[14] CMS Collaboration. "Phenomenological MSSM interpretation of CMS searches in pp collisions at $\sqrt{s} = 7$ and 8 TeV". In: *JHEP* 2016.10 (Oct. 2016). DOI: 10.1007/jhep10(2016)129. arXiv: 1606.03577 [hep-ex].

[15] G. Aad et al. "Summary of the ATLAS experiment's sensitivity to supersymmetry after LHC Run 1 — interpreted in the phenomenological MSSM". In: *Journal of High Energy Physics* 2015.10 (Oct. 2015). ISSN: 1029-8479. DOI: 10.1007/jhep10(2015)134. URL: http://dx.doi.org/10.1007/JHEP10(2015)134.

[16] V. Khachatryan et al. "Phenomenological MSSM interpretation of CMS searches in pp collisions at $\sqrt{s} = 7$and 8 TeV". In: *Journal of High Energy Physics* 2016.10 (Oct. 2016). ISSN: 1029-8479. DOI: 10.1007/jhep10(2016)129. URL: http://dx.doi.org/10.1007/JHEP10(2016)129.

[17] Carola F Berger et al. "Supersymmetry without prejudice". In: *Journal of High Energy Physics* 2009.02 (Feb. 2009), pp. 023–023. ISSN: 1029-8479. DOI: 10.1088/1126-6708/2009/02/023. URL: http://dx.doi.org/10.1088/1126-6708/2009/02/023.

[18] Matthew W. Cahill-Rowley et al. "The new look pMSSM with neutralino and gravitino LSPs". In: *The European Physical Journal C* 72.9 (Sept. 2012). ISSN: 1434-6052. DOI: 10.1140/epjc/s10052-012-2156-1. URL: http://dx.doi.org/10.1140/epjc/s10052-012-2156-1.

[19] Ursula Laa. *On the coverage of the pMSSM by simplified model results*. 2017. arXiv: 1709.10386 [hep-ph].

[20] S. S. AbdusSalam et al. "Benchmark Models, Planes, Lines and Points for Future SUSY Searches at the LHC". In: *Eur. Phys. J. C* 71 (2011), p. 1835. DOI: 10.1140/epjc/s10052-011-1835-7. arXiv: 1109.3859 [hep-ph].

[21] W. Porod. "SPheno, a program for calculating supersymmetric spectra, SUSY particle decays and SUSY particle production at e+e- colliders". In: *Computer Physics Communications* 153.2 (2003), pp. 275–315. ISSN: 0010-4655. DOI: https://doi.org/10.1016/S0010-4655(03)00222-4. URL: https://www.sciencedirect.com/science/article/pii/S0010465503002224.

[22] W. Porod and F. Staub. "SPheno 3.1: extensions including flavour, CP-phases and models beyond the MSSM". In: *Computer Physics Communications* 183.11 (Nov. 2012), pp. 2458–2469. ISSN: 0010-4655. DOI: 10.1016/j.cpc.2012.05.021. URL: http://dx.doi.org/10.1016/j.cpc.2012.05.021.

[23] P Skands et al. "SUSY Les Houches Accord: Interfacing SUSY Spectrum Calculators, Decay Packages, and Event Generators". In: *Journal of High Energy Physics* 2004.07 (July 2004), pp. 036–036. ISSN: 1029-8479. DOI: 10.1088/1126-6708/2004/07/036. URL: http://dx.doi.org/10.1088/1126-6708/2004/07/036.

[24] Anthony O'Hagan and Jonathan J. Forster. *Kendall's Advanced Theory of Statistics, volume 2B: Bayesian Inference*. Vol. 2B. London: Arnold, 1994.

[25] A. A. Markov. *Extension of the limit theorems of probability theory to a sum of variables connected in a chain*. reprinted in Appendix B of: R. Howard, *Dynamic Probabilistic Systems, volume 1: Markov Chains*. John Wiley and Sons, 1971.

[26] N. Metropolis et al. "Equation of state calculations by fast computing machines". In: *J. Chem. Phys 21* 1087 (1953). DOI: 10.1063/1.1699114.

[27] W. K. Hastings. "Monte Carlo sampling methods using Markov chains and their applications". In: *Biometrika* 12.97 (1970). DOI: 10.1093/biomet/57.1.97.

[28] B. A. Berg. *Markov chain Monte Carlo simulations and their statistical analysis*. Singapore: World Scientific, 2004.

[29] Henning Bahl et al. *Precision calculations in the MSSM Higgs-boson sector with FeynHiggs 2.14*. 2019. arXiv: 1811.09073 [hep-ph].

[30] Henning Bahl et al. "Reconciling EFT and hybrid calculations of the light MSSM Higgs-boson mass". In: *The European Physical Journal C* 78.1 (Jan. 2018). ISSN: 1434-6052. DOI: 10.1140/epjc/s10052-018-5544-3. URL: http://dx.doi.org/10.1140/epjc/s10052-018-5544-3.

[31] Henning Bahl and Wolfgang Hollik. "Precise prediction for the light MSSM Higgs-boson mass combining effective field theory and fixed-order calculations". In: *The European Physical Journal C* 76.9 (Sept. 2016). ISSN: 1434-6052. DOI: 10.1140/epjc/s10052-016-4354-8. URL: http://dx.doi.org/10.1140/epjc/s10052-016-4354-8.

[32] T. Hahn et al. "High-Precision Predictions for the LightCP-Even Higgs Boson Mass of the Minimal Supersymmetric Standard Model". In: *Physical Review Letters* 112.14 (Apr. 2014). ISSN: 1079-7114. DOI: 10.1103/physrevlett.112.141801. URL: http://dx.doi.org/10.1103/PhysRevLett.112.141801.

[33] Meikel Frank et al. "The Higgs boson masses and mixings of the complex MSSM in the Feynman-diagrammatic approach". In: *Journal of High Energy Physics* 2007.02 (Feb. 2007), pp. 047–047. ISSN: 1029-8479. DOI: 10.1088/1126-6708/2007/02/047. URL: http://dx.doi.org/10.1088/1126-6708/2007/02/047.

[34] G. Degrassi et al. "Towards high-precision predictions for the MSSM Higgs sector". In: *The European Physical Journal C* 28.1 (May 2003), pp. 133–143. ISSN: 1434-6052. DOI: 10.1140/epjc/s2003-01152-2. URL: http://dx.doi.org/10.1140/epjc/s2003-01152-2.

[35] S. Heinemeyer, W. Hollik, and G. Weiglein. "The masses of the neutral $\mathcal{CP}$ -even Higgs bosons in the MSSM: Accurate analysis at the two-loop level". In: *The European Physical Journal C* 9.2 (June 1999), pp. 343–366. ISSN: 1434-6052. DOI: 10.1007/s100529900006. URL: http://dx.doi.org/10.1007/s100529900006.

[36] S. Heinemeyer, W. Hollik, and G. Weiglein. "FeynHiggs: a program for the calculation of the masses of the neutral -even Higgs bosons in the MSSM". In: *Computer Physics Communications* 124.1 (Jan. 2000), pp. 76–89. ISSN: 0010-4655. DOI: 10.1016/s0010-4655(99)00364-1. URL: http://dx.doi.org/10.1016/S0010-4655(99)00364-1.

[37] F. Mahmoudi. "SuperIso v2.3: A program for calculating flavor physics observables in supersymmetry". In: *Computer Physics Communications* 180.9 (Sept. 2009), pp. 1579–1613. ISSN: 0010-4655. DOI: 10.1016/j.cpc.2009.02.017. URL: http://dx.doi.org/10.1016/j.cpc.2009.02.017.

[38] Philip Bechtle et al. "HiggsSignals: Confronting arbitrary Higgs sectors with measurements at the Tevatron and the LHC". In: *The European Physical Journal C* 74.2 (Feb. 2014). ISSN: 1434-6052. DOI: 10.1140/epjc/s10052-013-2711-4. URL: http://dx.doi.org/10.1140/epjc/s10052-013-2711-4.

[39] Philip Bechtle et al. "HiggsSignals-2: Probing new physics with precision Higgs measurements in the LHC 13 TeV era". In: *Eur. Phys. J. C* 81.2 (2021), p. 145. DOI: 10.1140/epjc/s10052-021-08942-y. arXiv: 2012.09197 [hep-ph].

[40] P. Bechtle et al. "HiggsBounds: Confronting arbitrary Higgs sectors with exclusion bounds from LEP and the Tevatron". In: *Computer Physics Communications* 181.1 (Jan. 2010), pp. 138–167. ISSN: 0010-4655. DOI: 10.1016/j.cpc.2009.09.003. URL: http://dx.doi.org/10.1016/j.cpc.2009.09.003.

[41] Philip Bechtle et al. *Recent Developments in HiggsBounds and a Preview of HiggsSignals*. 2013. arXiv: 1301.2345 [hep-ph].

[42] Philip Bechtle et al. "HiggsBounds-4: improved tests of extended Higgs sectors against exclusion bounds from LEP, the Tevatron and the LHC". In: *The European Physical Journal C* 74.3 (Mar. 2014). ISSN: 1434-6052. DOI: 10.1140/epjc/s10052-013-2693-2. URL: http://dx.doi.org/10.1140/epjc/s10052-013-2693-2.

[43] Philip Bechtle et al. "Applying exclusion likelihoods from LHC searches to extended Higgs sectors". In: *The European Physical Journal C* 75.9 (Sept. 2015). ISSN: 1434-6052. DOI: 10.1140/epjc/s10052-015-3650-z. URL: http://dx.doi.org/10.1140/epjc/s10052-015-3650-z.

[44] Philip Bechtle et al. "HiggsBounds-5: Testing Higgs Sectors in the LHC 13 TeV Era". In: *Eur. Phys. J. C* 80.12 (2020), p. 1211. DOI: 10.1140/epjc/s10052-020-08557-9. arXiv: 2006.06007 [hep-ph].

[45] Peter Athron et al. "GM2Calc: precise MSSM prediction for $(g-2)$ of the muon". In: *The European Physical Journal C* 76.2 (Feb. 2016). ISSN: 1434-6052. DOI: 10.1140/epjc/s10052-015-3870-2. URL: http://dx.doi.org/10.1140/epjc/s10052-015-3870-2.

[46] Peter Athron et al. *Two-loop Prediction of the Anomalous Magnetic Moment of the Muon in the Two-Higgs Doublet Model with GM2Calc 2*. 2021. arXiv: 2110.13238 [hep-ph].

[47] B. Abi et al. "Measurement of the Positive Muon Anomalous Magnetic Moment to 0.46 ppm". In: *Physical Review Letters* 126.14 (Apr. 2021). ISSN: 1079-7114. DOI: 10.1103/physrevlett.126.141801. URL: http://dx.doi.org/10.1103/PhysRevLett.126.141801.

[48] Sabine Kraml et al. "SModelS: a tool for interpreting simplified-model results from the LHC and its application to supersymmetry". In: *Eur. Phys. J. C* 74 (2014), p. 2868. DOI: 10.1140/epjc/s10052-014-2868-5. arXiv: 1312.4175 [hep-ph].

[49] Federico Ambrogi et al. "SModelS v1.1 user manual: Improving simplified model constraints with efficiency maps". In: *Comput. Phys. Commun.* 227 (2018), pp. 72–98. DOI: 10.1016/j.cpc.2018.02.007. arXiv: 1701.06586 [hep-ph].

[50] Federico Ambrogi et al. "SModelS v1.2: long-lived particles, combination of signal regions, and other novelties". In: *Comput. Phys. Commun.* 251 (2020), p. 106848. DOI: 10.1016/j.cpc.2019.07.013. arXiv: 1811.10624 [hep-ph].

[51] Gaël Alguero et al. "New developments in SModelS". In: *PoS* TOOLS2020 (2021), p. 022. DOI: 10.22323/1.392.0022. arXiv: 2012.08192 [hep-ph].

[52] G. Bélanger et al. "micrOMEGAs$_3$: $A program for calculating dark matter observables$". In: *Computer Physics Communications* 185.3 (Mar. 2014), pp. 960–985. ISSN: 0010-4655. DOI: 10.1016/j.cpc.2013.10.016. URL: http://dx.doi.org/10.1016/j.cpc.2013.10.016.

[53] D. Barducci et al. *Collider limits on new physics within micrOMEGAs4.3*. 2017. arXiv: 1606.03834 [hep-ph].

[54] G. Bélanger et al. "Dark matter direct detection rate in a generic model with micrOMEGAs_2.2". In: *Computer Physics Communications* 180.5 (May 2009), pp. 747–767. ISSN: 0010-4655. DOI: 10.1016/j.cpc.2008.11.019. URL: http://dx.doi.org/10.1016/j.cpc.2008.11.019.

[55] LHC Higgs Cross Section Working Group et al. *LHC HXSWG interim recommendations to explore the coupling structure of a Higgs-like particle*. 2012. DOI: 10.48550/ARXIV.1209.0040. URL: https://arxiv.org/abs/1209.0040.

[56] C T Potter et al. *Handbook of LHC Higgs Cross Sections: 3. Higgs Properties: Report of the LHC Higgs Cross Section Working Group*. en. 2013. DOI: 10.5170/CERN-2013-004. URL: http://cds.cern.ch/record/1559921.

[57] H. Bahl et al. "HL-LHC and ILC sensitivities in the hunt for heavy Higgs bosons". In: *Eur. Phys. J. C* 80.10 (2020), p. 916. DOI: 10.1140/epjc/s10052-020-08472-z. arXiv: 2005.14536 [hep-ph].

[58] J. de Blas et al. "Higgs Boson studies at future particle colliders". In: *Journal of High Energy Physics* 2020.1 (Jan. 2020). DOI: 10.1007/jhep01(2020)139. URL: https://doi.org/10.1007%2Fjhep01%282020%29139.

[59] T. Aoyama et al. "The anomalous magnetic moment of the muon in the Standard Model". In: *Phys. Rept.* 887 (2020), pp. 1–166. DOI: 10.1016/j.physrep.2020.07.006. arXiv: 2006.04822 [hep-ph].

[60] Manimala Chakraborti, Sven Heinemeyer, and Ipsita Saha. "The new "MUON G-2" result and supersymmetry". In: *Eur. Phys. J. C* 81.12 (2021), p. 1114. DOI: 10.1140/epjc/s10052-021-09900-4. arXiv: 2104.03287 [hep-ph].

[61] Planck Collaboration: N. Aghanim et. al. "Planck 2018 results". In: *Astronomy & Astrophysics* 641 (Sept. 2020), A6. DOI: 10.1051/0004-6361/201833910. URL: https://doi.org/10.1051%2F0004-6361%2F201833910.

[62] Manimala Chakraborti, Sven Heinemeyer, and Ipsita Saha. "Improved $(g-2)_\mu$ measurements and wino/higgsino dark matter". In: *Eur. Phys. J. C* 81.12 (2021), p. 1069. DOI: 10.1140/epjc/s10052-021-09814-1. arXiv: 2103.13403 [hep-ph].

[63] S. Lloyd. "Least squares quantization in PCM". In: *IEEE Trans. Inf. Theory* 28.2 (1982), pp. 129–137. DOI: 10.1109/TIT.1982.1056489.

[64] Martin Ester et al. "A Density-Based Algorithm for Discovering Clusters in Large Spatial Databases with Noise". In: *Proceedings of the Second International Conference on Knowledge Discovery and Data Mining*. KDD'96. Portland, Oregon: AAAI Press, 1996, pp. 226–231.

[65] Robert Tibshirani, Walther Guenther, and Trevor Hastie. "Estimating the Number of Clusters in a Data Set via the Gap Statistic". In: . *J. R. Stat. Soc. B* (2001), pp. 411–423.

[66] ATLAS Collaboration. "Search for a scalar partner of the top quark in the all-hadronic $t\bar{t}$ plus missing transverse momentum final state at $\sqrt{s} = 13$ TeV with the ATLAS detector". In: *Eur. Phys. J. C* 80.8 (2020), p. 737. DOI: 10.1140/epjc/s10052-020-8102-8. arXiv: 2004.14060 [hep-ex].

A Coverage of the scan

Throughout this section, sampled pMSSM points that are excluded at post-processing are shown separately from the final accepted sample. Points accepted by the McMC but excluded at 95% CL by HiggsBounds (LHC Higgs searches) are shown in purple. Of the remaining points, those excluded at 95% CL by SModels (LHC SUSY searches) are shown in dark blue. And of the remaining points, those excluded at 95% CL by Micromegas (dark matter measurements) are shown in light blue. The green distribution shows the points that are fully accepted after all post-processing steps.

A.1 pMSSM parameters

The distribution of the sampled trilinear couplings (A_t, A_b, and A_l) are shown in Figure 16. The symmetry across 0 shows that the random selection of initial scan points does indeed populate all sign combinations effectively.

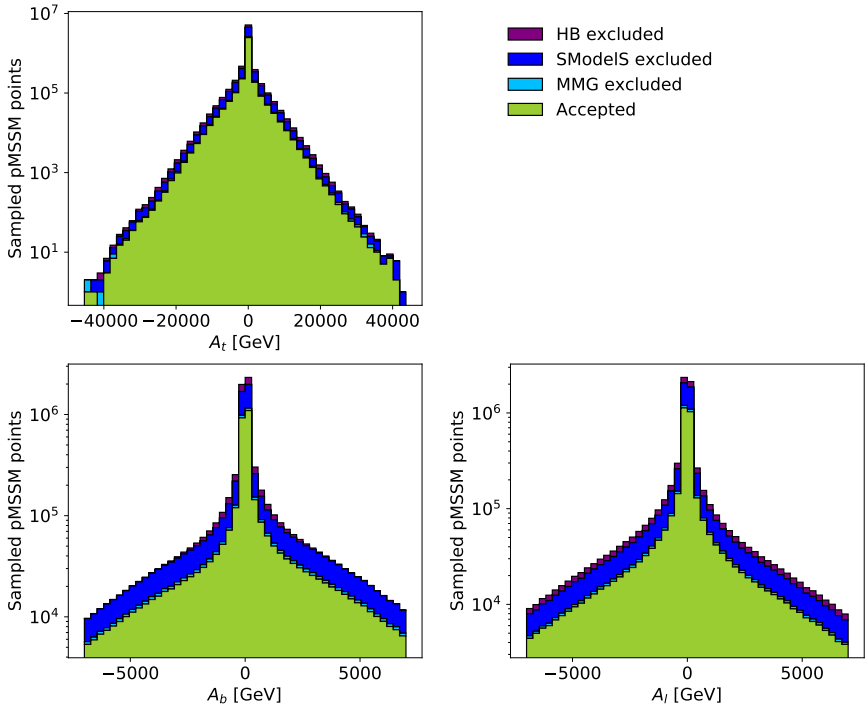

Figure 16: Distribution of the trilinear couplings A_t, A_b, and A_l of sampled pMSSM points.

The distributions of the sampled gaugino mass parameters (μ, M_1, M_2, and M_3) are shown in Figure 17. Again, good symmetry across 0 is observed in μ, M_1, and M_2. The power of LHC SUSY searches is visible at low values of these mass parameters, where the SModelS exclusion rules out the majority of points accepted by the McMC.

The sampled values of slepton mass parameters are shown in Figure 18 for left-handed (left) and right-handed (right) sleptons. The peak at low values of the smuon/selectron mass corresponds to those points with large Δa_μ. These are largely excluded by SModelS.

The sampled squark mass parameters are shown in Figure 19: the left column shows the right-handed up-type, the center column shows the right-handed down-type, and the right column shows the left-handed squark masses. Again, LHC searches have been able to exclude much of the parameter space at low squark masses, as showwn by the SModelS exclusion.

The pMSSM Higgs paramters, the mass of the heavy Higgs boson M_A and $\tan\beta$, are shown in Figure 20. HiggsBounds, which includes dedicated LHC searches for the decay of the heavy Higgs, and SModelS exclude all points with $M_A < 1$ TeV.

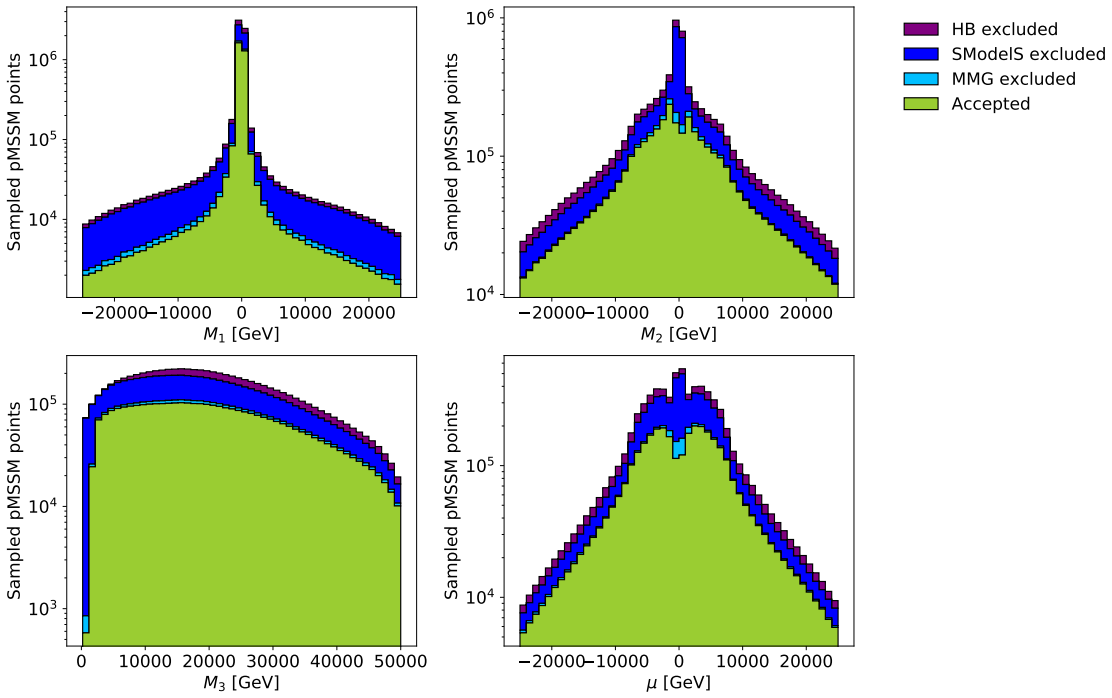

Figure 17: Distribution of the gaugino mass parameters M_3, M_1, M_2, and μ of sampled pMSSM points.

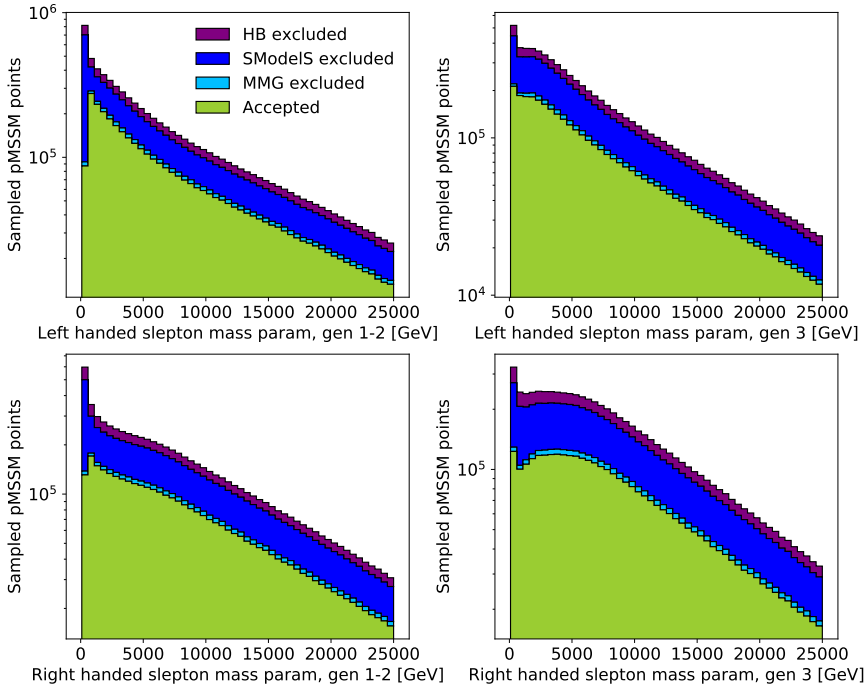

Figure 18: Distribution of slepton mass parameters $m_{\tilde{L}^{1,2}}$, $m_{\tilde{L}^3}$, $m_{\tilde{R}^{1,2}}$, and $m_{\tilde{R}^3}$ of sampled pMSSM points.

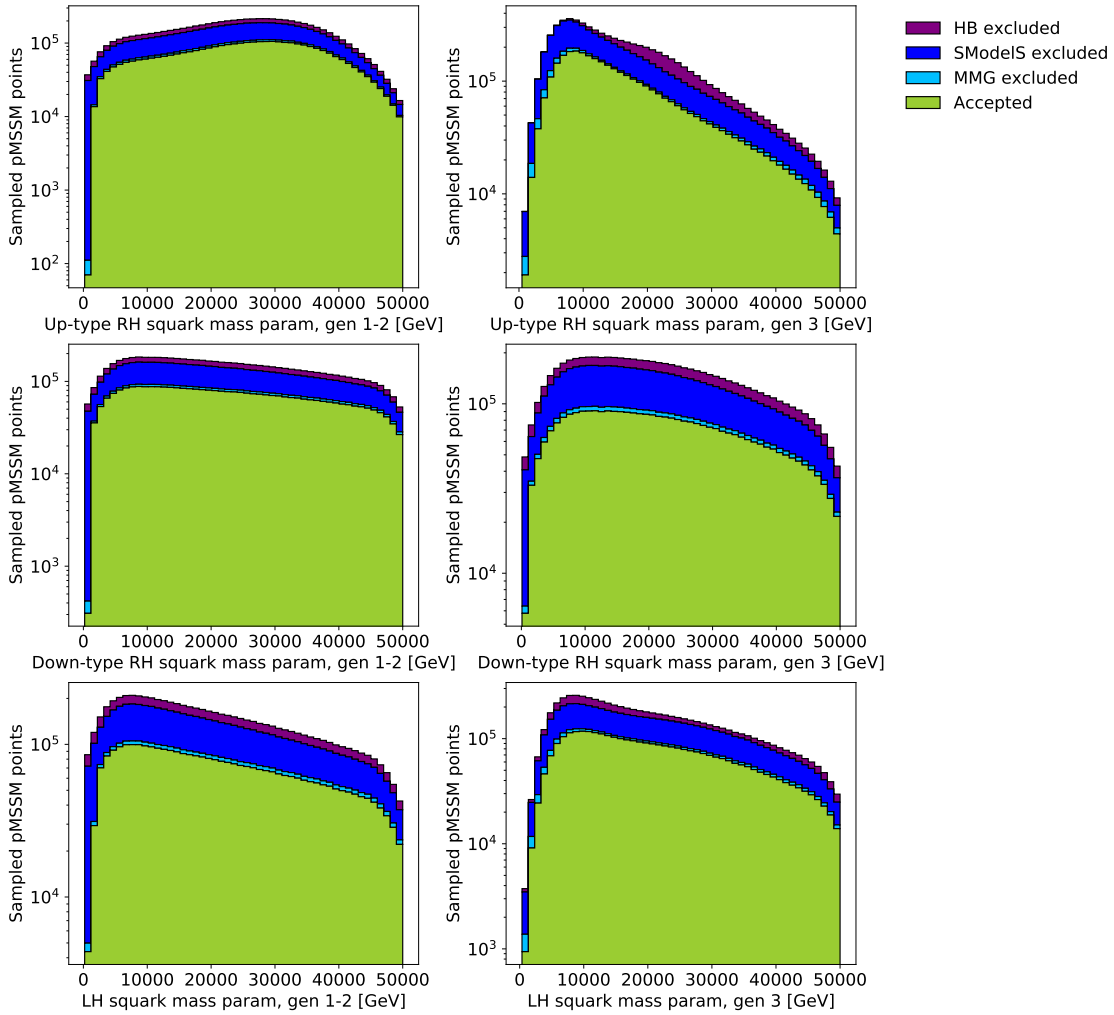

Figure 19: Distribution of squark mass parameters (left) $m_{\tilde{u}^{1,2}}$, $m_{\tilde{u}^3}$, (center) $m_{\tilde{d}^{1,2}}$, $m_{\tilde{d}^3}$, (right) $m_{\tilde{q}^{1,2}}$, $m_{\tilde{q}^3}$ of sampled pMSSM points.

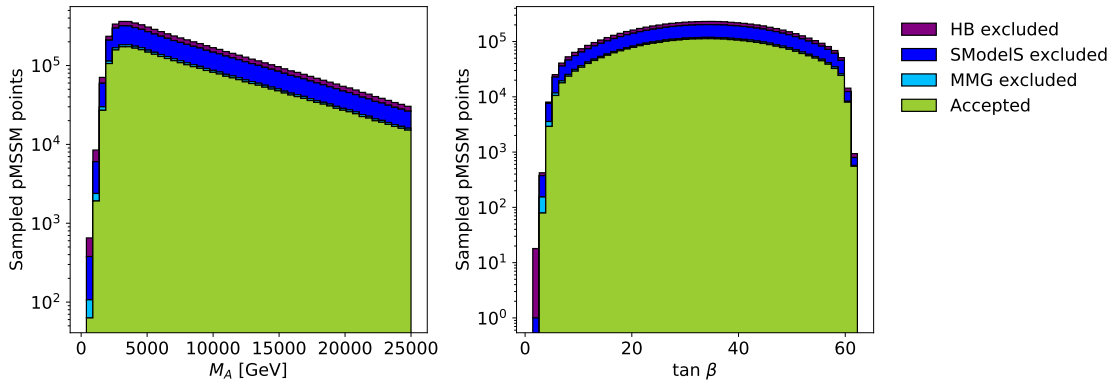

Figure 20: The sampled mass of the heavy Higgs boson M_A (left), and $\tan\beta$ (right) for the sampled pMSSM points.

A.2 Sparticle masses

This section shows the distributions of sparticle masses of the sampled pMSSM points. Figure 21 shows the slepton masses, and Figure 22 shows the sneutrino masses. Figure 23 shows the sbottom and stop quark masses, and Figure 24 shows the gluino mass. The neutralino and chargino masses are shown in Figures 25 and 26, respectively.

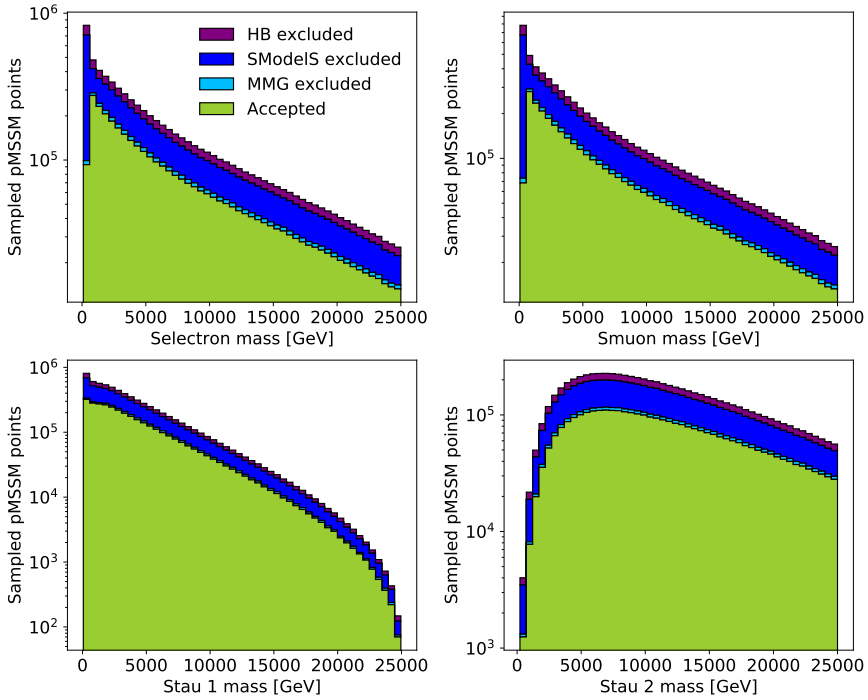

Figure 21: Slepton masses

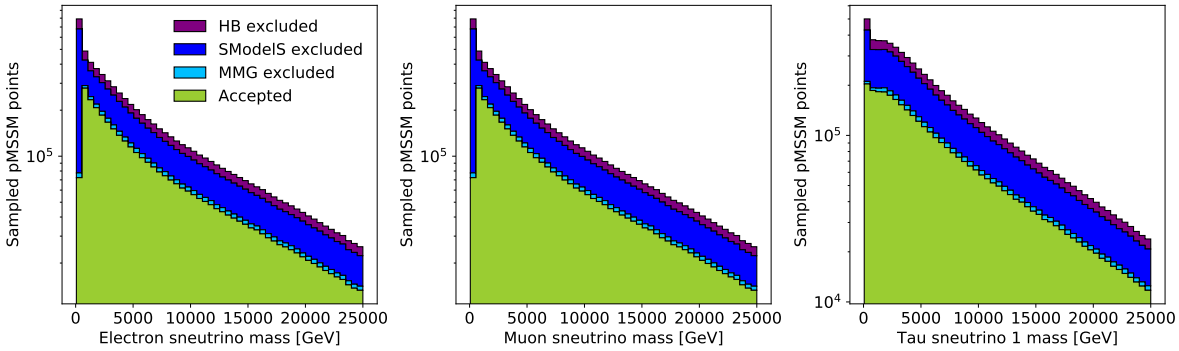

Figure 22: Sneutrino masses

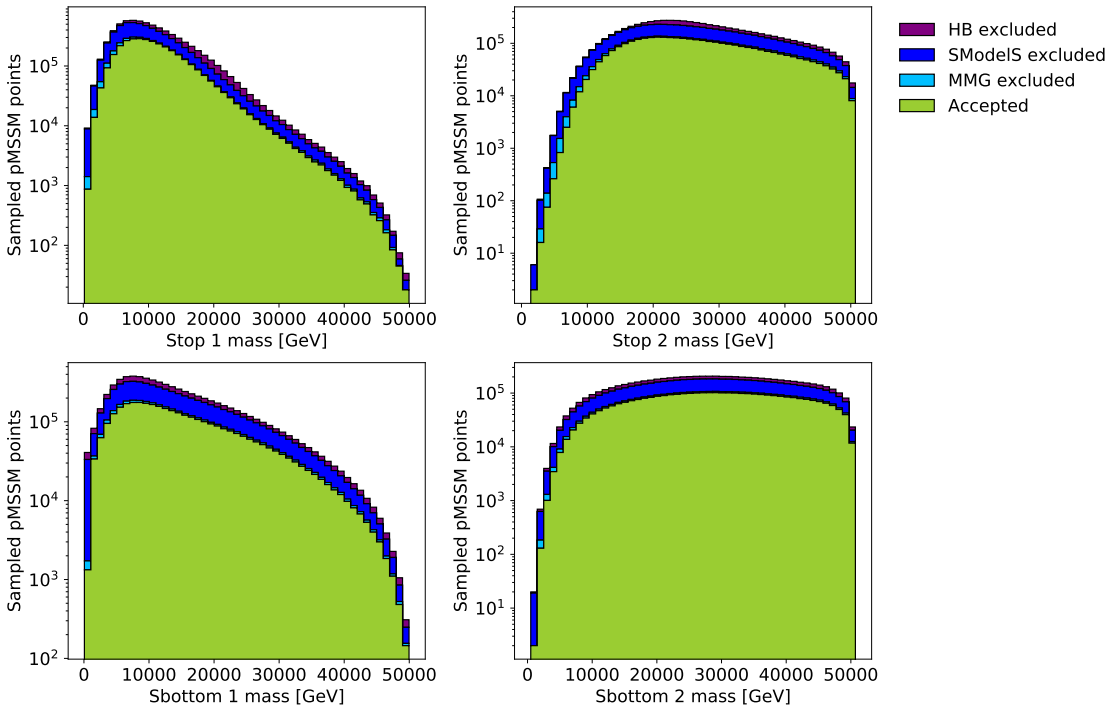

Figure 23: Heavy squark masses

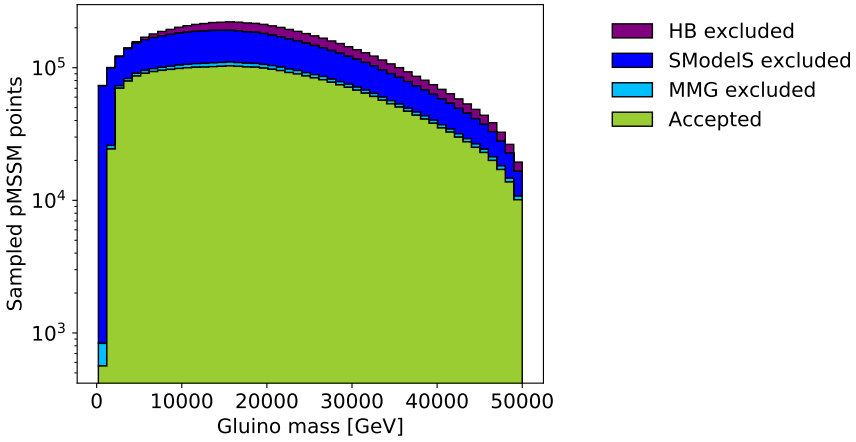

Figure 24: Gluino mass

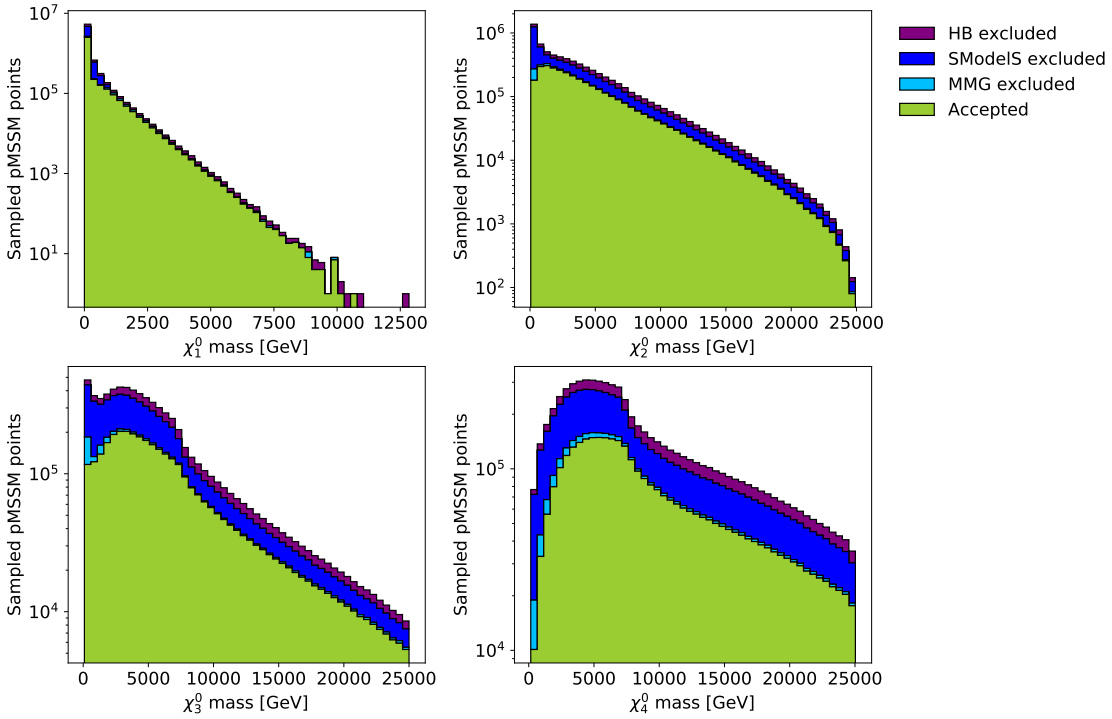

Figure 25: Neutralino masses

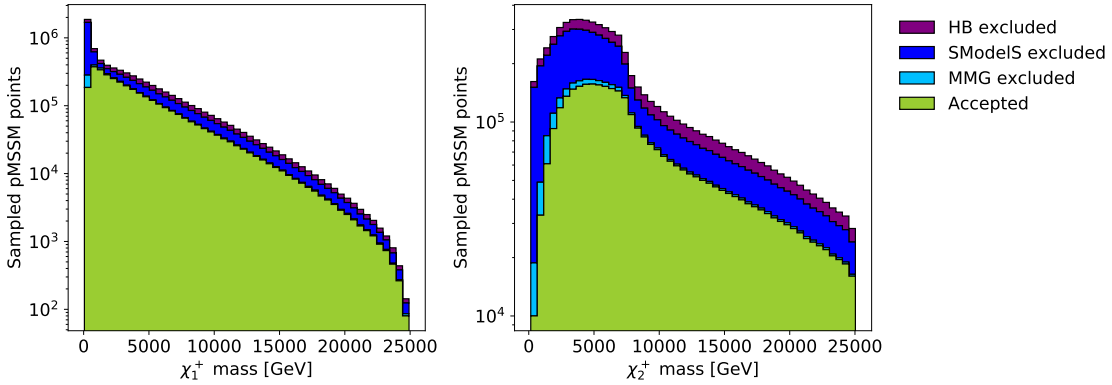

Figure 26: Chargino masses

A.3 Standard Model observables

The top and bottom quark masses, along with the strong coupling constant α_S, for each pMSSM point are shown in Figure 27.

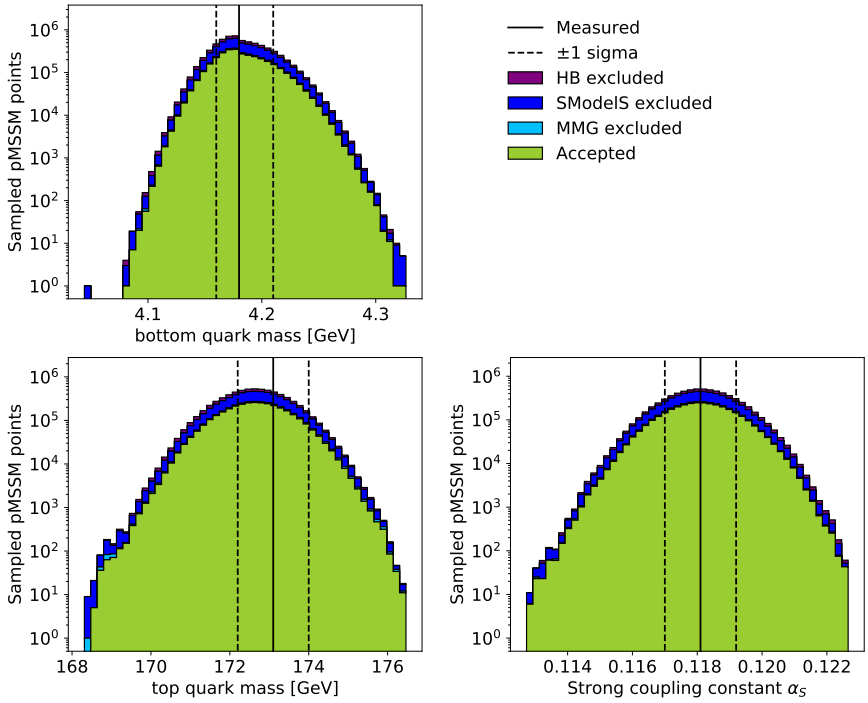

Figure 27: Strong coupling constant (left), bottom quark mass (center), and top quark mass (right) for each sampled pMSSM point, with the measured value and uncertainties indicated by vertical lines.